ACS OMEGA

http://pubs.acs.org/journal/acsodf

Article

Combustion Characteristic Prediction of a Supercritical CO_2 Circulating Fluidized Bed Boiler Based on Adaptive GWO-SVM

Ying Cui,* Ye Zou, Shujun Jiang, and Wenqi Zhong*

Cite This: *ACS Omega* 2023, 8, 10160−10175

Read Online

ACCESS | Metrics & More | Article Recommendations

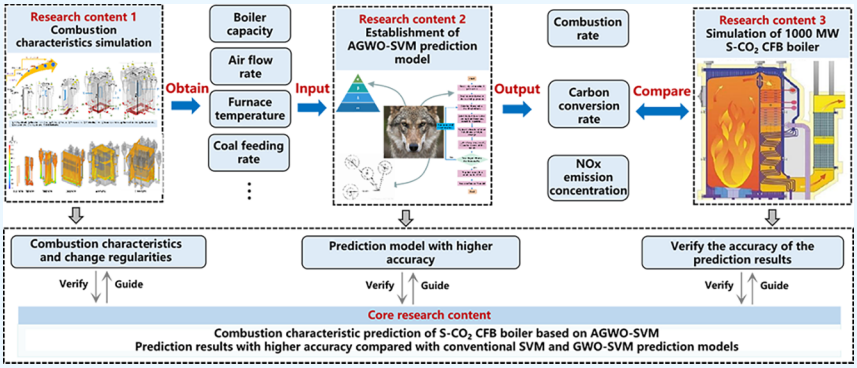

ABSTRACT: The development of a new and efficient supercritical carbon dioxide (S-CO_2) power cycle system is one of the important technical ways to break through the bottleneck of coal power development, improve the efficiency of power generation, and realize energy saving and emission reduction. In order to simplify the complicated workload and save the huge time cost of numerical simulations on combustion characteristics, it is of great significance to accurately make the combustion characteristic prediction according to the operating performance of the S-CO_2 CFB boiler. This study proposed a combustion characteristic prediction model corresponding to the S-CO_2 CFB boiler based on the adaptive gray wolf optimizer support vector machine (AGWO-SVM). The parameters of the gray wolf optimizer algorithm were processed adaptively first combined with the boiler characteristics, and then the adaptive gray wolf optimizer algorithm was integrated with the support vector machine to solve the imbalance of local and global search problems of particles being easy to gather in a certain position in the process of pattern recognition. The novel method effectively predicts the boiler in the scaling process from the aspect of boiler capacity, optimizes the combustion characteristic expression by numerical simulations, greatly saves time cost and applicability of enlarged design by altering complex numerical simulations, and lays the application foundation of the S-CO_2 CFB boiler in the industrial field with acceptable operation accuracy.

1. INTRODUCTION

The supercritical CO_2 (S-CO_2) power cycle has received extensive attention and research in the fields of nuclear energy, fossil, concentrated solar energy, waste heat recovery, and ship propulsion system due to its advantages, such as simple system structure, high cycle efficiency, compact components, and environmental friendliness.[1−3] In the coal-fired power generation field, circulating fluidized bed (CFB) coal-fired power generation technology, as the most industrialized clean coal combustion technology, has advantages of low NO_x emission, simple desulfurization process, high combustion efficiency, and wide coal applicability compared with the pulverized boiler.[4−7] The combination of CFB coal-fired power generation technology with the S-CO_2 power cycle has attracted wide attention from scholars all over the world.[8−11] The heat transfer temperature of S-CO_2 working fluid ranging from 530 to 650 °C is about 150 °C higher than that of the conventional steam (330−600 °C), which improves the boundary temperature of the furnace, enhances the furnace combustion process and the heat transfer of the heating surfaces, and improves the combustion efficiency and carbon conversion rate of the boiler.[12,13]

Combustion and heat transfer characteristics of S-CO_2 CFB boilers change significantly compared with traditional steam CFB boilers, which brings new challenges to the high efficiency and low pollution combustion and regulation of the boiler. Xu

Received: November 22, 2022
Accepted: February 27, 2023
Published: March 8, 2023

et al.[9] summarized the thermal coupling relationship between the S-CO_2 power cycle and coal-fired boilers, among which the most important is that using the S-CO_2 working medium cycle instead of water steam as the heat transfer boundary affects the combustion characteristics and pollutant generation process in the furnace. On the one hand, due to the unique physical and thermal properties of CO_2, the boundary conditions of the coal-fired S-CO_2 CFB boiler are different from those of the conventional steam CFB boiler, and the boiler structure and heating surface layout have changed.[14] On the other hand, the temperature of the S-CO_2 working medium into the coal-fired boiler (about 530 °C) is much higher than that of the steam cycle temperature (about 233 °C),[6] which affects the heat transfer surface temperature distribution and heat flux distribution, resulting in the furnace combustion characteristics, heat transfer performance, and pollutant emission characteristics far from the traditional steam ones.

In order to master the combustion characteristics under the unique heat transfer boundary of S-CO_2, many scholars and scientific research units all over the world have made great efforts.[15,16] Zhou et al.[17] analyzed the fuel combustion loss rate of the 1000 MW S-CO_2 Brayton cycle coal-fired power generation system and proposed better system operating parameters. Yang et al.[18] simulated the combustion process of the 300 MW S-CO_2 pulverized coal boiler coupled with the heat transfer process of the working medium, and it was found that the two peak temperature regions of the spiral wall heater were about 900 K. Wang et al.[19] established the S-CO_2 one-dimensional fluid dynamics model and conducted the numerical simulation of a 5 MW gas S-CO_2 test boiler combined with the CFD simulation method. Gu et al.[20] focused on a 12 MW pilot S-CO_2 CFB boiler under oxy-fuel by 3D CFD numerical simulation, and the influence of different heat transfer boundary conditions and different oxygen concentrations on the particle movement, combustion characteristics, and gas pollutant emission characteristics was systematically studied.

In the process of enlarging the boiler capacity and operating parameters of the S-CO_2 CFB boiler, the change regularities of combustion characteristics of the furnace are complex, which is affected by various factors such as furnace structure design, size, air flow rate, and coal feeding rate.[11,21] Meanwhile, the complexity of the high-concentration gas−solid two-phase flow of the circulation process will take high time cost and have limitations to relying entirely on numerical simulation. Therefore, it is of great significance to accurately predict the combustion characteristics according to the working conditions and operating characteristics of the industrial S-CO_2 CFB boiler.

It is difficult to establish an accurate prediction model of the combustion characteristics of the S-CO_2 CFB boiler based on the conventional analytic formula modeling method. In recent years, the rapid development of artificial intelligence technology has been extensively used in China and abroad. Among them, the support vector machine (SVM), which is an important machine learning method to develop an intelligent diagnosis system, has attracted considerable attention in recent years. Its strong generalization ability makes it more and more commonly used in the field of coal-fired power generation.[22−26] Gu and Liu[27] proposed an SVM based on an improved particle swarm algorithm (IPSO-SVM) prediction model, which improves the motion pattern recognition rate of signals. Combined with the characteristics of the Gallic smelting production process, the accuracy is significantly better than the traditional SVM and PSO-SVM models. Zhang et al.[25] established NO_x emission, fly ash carbon content, and flue gas temperature models based on a least square-support vector machine (LS-SVM) to effectively improve boiler efficiency and reduce noise emissions through combustion optimization. The SVM seeks the optimal classification surface for the linear stability of sample data in high-dimensional space, and its calculation and storage data are not limited by the input dimension, which conforms to the characteristics of many factors affecting the combustion characteristics of S-CO_2 CFB boilers.[28−30] The gray wolf optimizer (GWO) algorithm is a new group intelligent optimization algorithm proposed according to the wolf hunting behavior and internal hierarchy. This algorithm solves a large number of continuous optimization problems with its fast convergence speed and high solution accuracy, and it has certain applications in combinatorial optimization problems.[31−34]

This study presents a combustion characteristic prediction model of the S-CO_2 CFB boiler based on an adaptive gray wolf optimizer support vector machine (AGWO-SVM). The parameters of the GWO algorithm were processed adaptively first combined with the boiler characteristics, and then the adaptive GWO algorithm was integrated with the SVM to solve the "precocious" convergence problem of particles being easy to gather in a certain position in the process of pattern recognition. The novel method predicts the boiler combustion efficiency, carbon conversion rate, and NO_x emission concentration with the boiler capacity increasing by comparing with the conventional prediction method and the original simulation data.

2. ESTABLISHMENT OF THE GWO-SVM PREDICTION MODEL

2.1. SVM. The SVM is a novel machine learning method proposed by the famous scholar V.N. Vapnik based on the Vapnik−Chervonenkis dimension theory and structural risk minimum principle of statistical learning. Its core idea is to transform the nonlinear data to the high-dimensional linear space and to meet the maximum classification spacing, so that the classification line can correctly separate the two types of samples, and then obtain the required optimal classification hyperplane. Assuming a dataset of $\{x_i, y_i\}$, $i = 1, 2, ..., N$, $y_i \in \{-1, +1\}$, $x_i \in R^d$ is given, the plane representing the two samples is classified by circles and forks, respectively.

When the SVM introduces the relaxation variable $\xi_i \geq 0$ and the penalty coefficient C' ($C' > 0$), the solution formula for the hyperplane is

$$\max \sum_{i=1}^{m} \alpha_i - \frac{1}{2}\sum_{i=1}^{m} \alpha_i \alpha_j y_i y_j (x_i, x_j)$$
$$\text{s. t. } 0 \leq \alpha_i \leq C', i = 1, \cdots, m$$
$$\sum_{i=1}^{m} \alpha_i y_i = 0 \quad (1)$$

where α_i is the Lagrangian factor solved by the quadratic optimization problem, and the optimal classification hyperplane is

https://doi.org/10.1021/acsomega.2c07483
ACS Omega 2023, 8, 10160−10175

$$f(x) = \text{sign}\left[\sum_{i=1}^{N} \alpha_i y_i (x_i \cdot x) + b\right] \quad (2)$$

When the raw data is nonlinear, the nuclear function is introduced for replacement, and the radial base nuclear function is generally used in the data processing of the S-CO_2 CFB boiler.

$$K(x, x') = \exp\left(-\frac{\|x - x'\|^2}{\sigma^2}\right) \quad (3)$$

Then, the optimal classification hyperplane is

$$f(x) = \text{sign}\left[\sum_{i=1}^{N} \alpha_i y_i k(x_i \cdot x) + b\right] \quad (4)$$

2.2. GWO. The GWO algorithm is proposed by the Australian scholar Mirjalili and coworkers in 2014, inspired by the wolf pack feeding process.[35] The GWO algorithm has the advantages of fast convergence speed, few parameters, simple principle, and being easy to implement.[36−38]

The GWO algorithm is an optimization algorithm inspired by the process of wolf search and hunting prey. As a social animal, wolves usually exist in nature and each population has a strict population system. In the group ranks according to the individual ability of the gray wolf, the most capable and highest individual α wolf with the highest level leads the whole population. The second β wolf is the executor of the α wolf command. The third level is δ wolf commanded by α wolf and β wolf, and the rest of the pack is ω wolf, which is the lowest level individual of the pack, as shown in Figure 1.

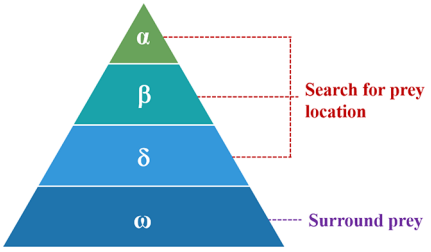

Figure 1. Level diagram of the GWO algorithm.

When rounding up prey, α wolf, β wolf, and δ wolf have the ability to search the prey position, while ω wolf rounds up the prey according to the position of α wolf, β wolf, and δ wolf. The GWO algorithm is mainly divided into search, surround, and capture with the mathematical model of the algorithm as follows:

(1) Search and surround. α wolf, β wolf, and δ wolf judge the direction of the prey and the distance from the prey according to the smell of the prey and guide ω wolf to surround the prey.

The distance between the prey and any individual gray wolf is described by D in eq 5.

$$D = |C' \cdot X_p(t) - X(t)| \quad (5)$$

where t represents iterations, $X_p(t)$ represents the prey location, $X(t)$ represents the location of ω wolf, and C' represents the coefficient vector with the range of [0,2]. The function of C' is to randomly adjust the difficulty of gray wolves close to the prey, so as to avoid the algorithm falling into the local optimum and better complete the optimization. When C' is less than 1, and when C' is greater than 1, it is more difficult to approach the prey, which is listed in eq 6.

$$C' = 2r_1 \quad (6)$$

where r_1 represents a random quantity ranging from 0 to 1.

The equation for a gray wolf to update the position is displayed as follows:

$$X(t + 1) = X_p(t) - A' \cdot D \quad (7)$$

where A' is the coefficient vector as listed in eq 8, whose value shows the gray wolf's exploration ability. When $|A'| > 1$, the gray wolf group will expand the search range and conduct a global search, and when $|A'| < 1$, the gray wolf group will shrink the search range for local accurate search.

$$A' = 2ar_2 - a \quad (8)$$

$$a = 2 - 2\frac{t}{\text{MaxIter}} \quad (9)$$

where r_2 is a random quantity with the range of [0,1], a represents the convergence factors that determine the search range, and MaxIter determines the maximum number of iterations indicating a linear decrease from 2 to 0 with iteration number t.

(2) Capture. Since the prey location (optimal solution) is unknown in the algorithm, and α wolf, β wolf, and δ wolf respectively represent the three positions closest to the prey, the prey location of the GWO algorithm is the position of α wolf, β wolf, and δ wolf, and ω wolf constantly updates its position according to the position of the three wolves and finally completes the capture.

$$D_\alpha = |C_1' \cdot X_\alpha(t) - X(t)| \quad (10)$$

$$D_\beta = |C_2' \cdot X_\beta(t) - X(t)| \quad (11)$$

$$D_\delta = |C_3' \cdot X_\delta(t) - X(t)| \quad (12)$$

$$X_1 = X_\alpha - A_1' \cdot D_\alpha \quad (13)$$

$$X_2 = X_\beta - A_2' \cdot D_\beta \quad (14)$$

$$X_3 = X_\delta - A_3' \cdot D_\delta \quad (15)$$

$$X_p(t + 1) = \frac{X_1 + X_2 + X_3}{3} \quad (16)$$

where D_α, D_β, and D_δ represent the distance between these three wolves and the ω wolf. $X_\alpha(t)$, $X_\beta(t)$, and $X_\delta(t)$ represent the positions of α wolf, β wolf, and δ wolf when the number of iterations is t, respectively. The position update formula of the ω wolf and the other three gray wolves is shown in eq 16.

The GWO algorithm completes the optimization according to the natural gray wolf hierarchy and the feeding process, which has the advantages of simple structure, few parameters, and being easy to realize. Compared with the GWO algorithm and genetic algorithm, the GWO algorithm optimization ability is stronger. However, the GWO algorithm itself also has shortcomings, such as the setting of the original convergence factor, so it needs to be improved adaptively.

2.3. AGWO-SVM. The prediction process of the combustion characteristics of the S-CO_2 CFB boiler focuses on optimizing the original convergence factor a in order to

https://doi.org/10.1021/acsomega.2c07483
ACS Omega 2023, 8, 10160−10175

expand the search range of the optimization in the early stage of the search and narrow the search range in the later stage for partial optimization. This treatment method solves the imbalance of local and global search problems of particles being easy to gather in a certain position in the process of pattern recognition. Local optimum means that the solution to a problem is optimal in a certain range or region, or to solve the problem or to achieve the goal is optimal within a certain range or limit. In some engineering fields, limited by time and cost, the local optimum and the global optimum may not be strictly checked, but in some cases, the formula requires the global optimum, which is to avoid the result of only the local optimum.

$$a = \frac{(a_{\text{initial}} - a_{\text{final}})}{2} + \cos\left(\frac{t}{\text{MaxIter}}\pi\right) \tag{17}$$

Figure 2 shows the comparison of convergence factor a before and after adaptive processing. It is seen that in the first

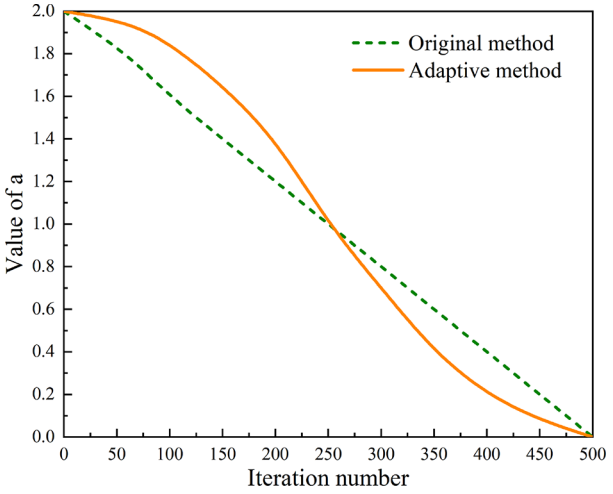

Figure 2. Comparison of convergence factor a before and after adaptive processing.

half of the iteration, adaptive a is always larger than the original a and the value of adaptive A is also larger than the original A. Compared with the previous iteration process of the original GWO algorithm, the scope of each time has strengthened the optimization ability of the algorithm. In the late iteration, after the adaptive processing of the convergence factor, the value of A is also smaller than the value of the original convergence factor. Therefore, the improved convergence factor strengthens the local search ability in the later period of optimization and the convergence accuracy of optimization is higher.

In addition, this study also introduces the dynamic weight strategy[39] to speed up the convergence speed of the GWO algorithm. Equation 16 is the position of the next update calculated by the GWO algorithm according to the position of α wolf, β wolf, and δ wolf. It is seen from the formula that α wolf, β wolf, and δ wolf lack pertinence in the guiding significance of wolves. Ignoring the different abilities of α wolf, β wolf, and δ wolf, the convergence speed of the algorithm is slow. In view of the defect of the GWO algorithm, the dynamic proportional weight mechanism is introduced, which makes α wolf have the largest influence on the next position update, with β wolf and δ wolf in order. The algorithm convergence is accelerated by introducing this strategy. The specific formula is listed from eqs 18 to 21.

$$W_\alpha = \frac{f_\alpha}{f_\alpha + f_\beta + f_\delta} \tag{18}$$

$$W_\beta = \frac{f_\beta}{f_\alpha + f_\beta + f_\delta} \tag{19}$$

$$W_\delta = \frac{f_\delta}{f_\alpha + f_\beta + f_\delta} \tag{20}$$

$$X_p(t+1) = \frac{X_1 \cdot W_1 + X_2 \cdot W_2 + X_3 \cdot W_3}{3} \tag{21}$$

where W_α, W_β, and W_δ represent the weight α wolf, β wolf, and δ wolf guide for the update of the ω wolf location, respectively, and f_α, f_β, and f_δ represent fitness values for each iteration of α wolf, β wolf, and δ wolf.

The AGWO algorithm improves on the penalty factor and kernel function parameters in the SVM, and then the two parameters obtained by the optimization are used as the SVM model. Figure 3 shows the flowchart of the AGWO-SVM algorithm. Specific steps are performed as listed below:

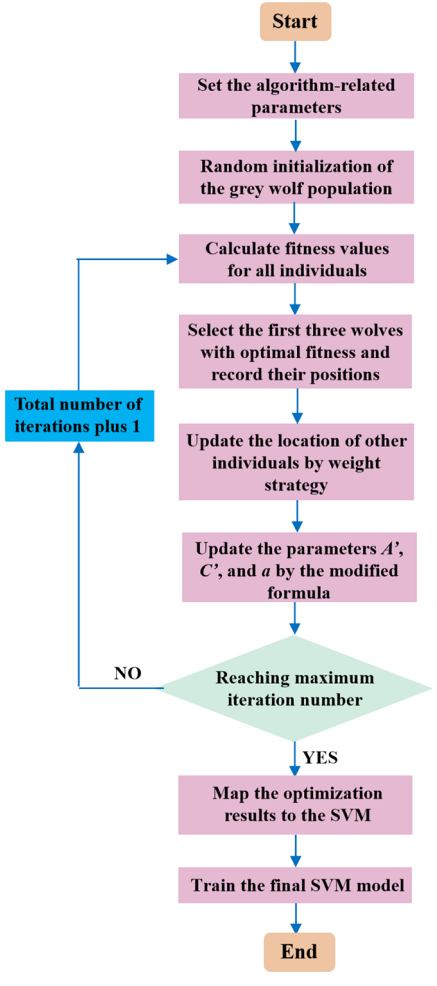

Figure 3. AGWO-SVM algorithm process.

https://doi.org/10.1021/acsomega.2c07483
ACS Omega 2023, 8, 10160−10175

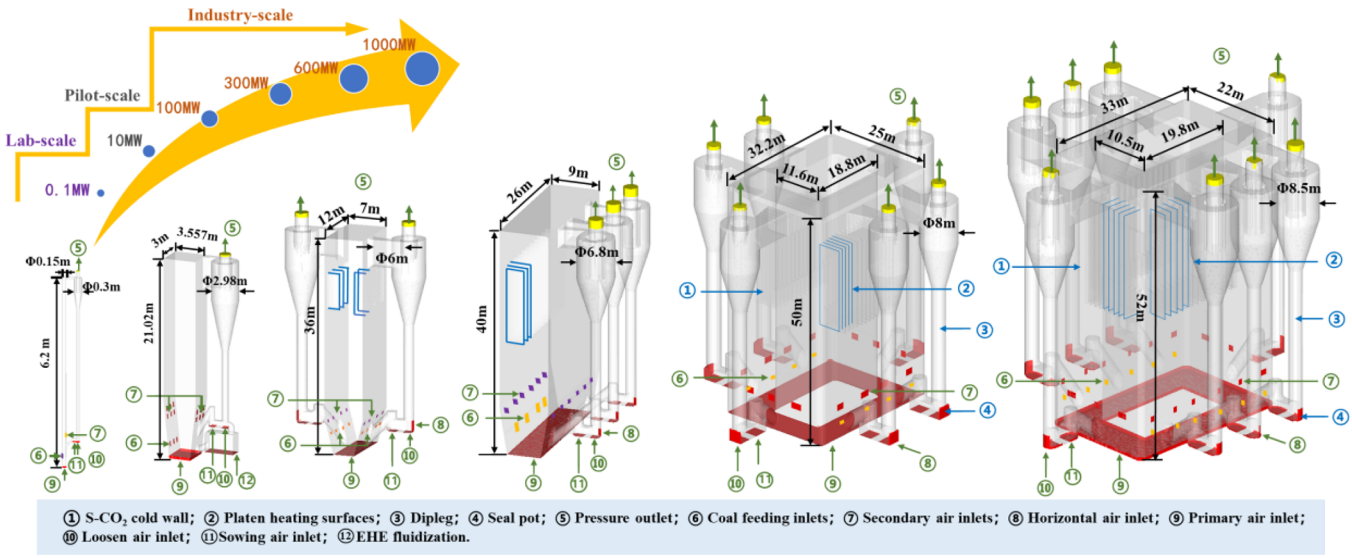

Figure 4. Physical models of lab-scale, pilot-scale, and industry-scale S-CO_2 CFB boilers.

Table 1. Input Parameters and Characteristic Parameters

operating parameters	0.1 MW	10 MW	100 MW	300 MW	600 MW	1000 MW
coal input (kg/s)	0.005	0.489	14.697	35.55	72.116	151.67
cold wall (K)	890	890.15	908.3	915.5	923.3	935.2
platen heating surfaces (K)			810.05	845.6	850.13	860.5
external heat exchanger (K)		810.5				
fluidization air temperature (K)	763	763	763	763	763	763
particle and gas						
diameter of bed material (mm)	0.2−0.6					
diameter of coal (mm)	0.01−5					
particle density (kg/m^3)	2400					
initial particle number	5.3×10^5	1.5×10^6	4.56×10^6	5.26×10^6	5.74×10^6	6.05×10^6
gas density (kg/m^3)	1.173					
gas viscosity (kg/m·s)	1.844×10^{-5}					
characteristic parameters						
excess air ratio	1.25	1.25	1.25	1.25	1.25	1.25
fluidization gas velocity (m/s)	2.8	3	3.56	4.2	4.5	5.5
residence time of gas (s)	2.48	6.9	8.28	9.56	10.11	12.5
volumetric thermal load (MW/m^3)	1.619	0.201	0.101	0.084	0.058	0.055
cross-sectional thermal load (MW/m^2)	10.04	4.23	3.63	3.37	2.9	2.85

(1) Relevant parameters such as population number, maximum number of iterations, and population size are set.
(2) Parameter initialization. Relevant parameters such as A', C', and a are initialized.
(3) The feature vectors obtained after data preprocessing are input into the SVM model for training.
(4) The fitness values of all gray wolves in the population are calculated and ranked in descending order to select α wolf, β wolf, and δ wolf.
(5) The position of the ω wolf is updated according to eqs 11−16.
(6) C' is updated according to eq 6, and A' is updated according to eqs 8 and 9.
(7) The fitness values of all gray wolves in the population and sort are counted. Compared with the last iteration, the three optimal values are found. When MaxIter is reached, the iteration of the algorithm stops and X_α is output. Otherwise, return to step (3) to recalculate.
(8) The SVM classification model is constructed by using the position of α wolf X in different dimensions as the value of the penalty factor and kernel function parameters in the SVM model.

3. PREDICTION MODEL OF BOILER COMBUSTION CHARACTERISTICS

3.1. Physical Model of S-CO_2 CFB Boilers. Full-loop CFD numerical simulation results of three-scale S-CO_2 CFB boilers with the capacity of 0.1, 10, 100, 300, 600, and 1000 MW, respectively, offer the database adopted in the prediction model. Figure 4 shows the physical model of the full-loop six-capacity S-CO_2 CFB boilers, and the authors' previous research[38] provides specific numerical simulation research methods, simulation processes, and combustion characteristic results. Based on the coal-fired CFB boiler design principle in accordance with the first law of thermodynamics and heat transfer law, the configuration and size for the six-capacity boilers are determined and designed. The six-capacity S-CO_2

https://doi.org/10.1021/acsomega.2c07483
ACS Omega 2023, 8, 10160−10175

CFB boilers consist of furnace main body, cyclone separator, S-CO_2 cold wall, dipleg, and seal pot. Different from the lab-scale boiler, the industry-scale boiler installs the platen heating surfaces inside the furnace and the pilot-scale boiler adds an external heat exchanger (EHE) because combustion releases more heat needing to be transferred. The primary air, the secondary air, and coal enter the furnace evenly from the bottom distribution plate, the secondary air inlets, and the coal feeding inlets arranged on the side wall of the lower furnace, respectively. Besides, the horizontal air, sowing air, and loosen air are designed at the seal pot position to make the bed material circulate more smoothly from the cyclones to the furnace. The furnace outlet is set as the pressure outlet boundary condition. Six S-CO_2 CFB boilers of different capacities are designed with the same regulation and belong to the same collective group with the detailed input parameters and characteristic parameters listed in Table 1.[11]

This study establishes the physical model of the 1000 MW S-CO_2 CFB boiler for numerical simulation of the gas−solid combustion process according to the same numerical simulation method introduced in the authors' previous research.[11] The purpose of simulating the 1000 MW S-CO_2 CFB boiler is to verify the accuracy of the combustion characteristics obtained based on the other five-capacity CFB boilers and to correct the scale-up fitting formulas as well. Besides, the accuracy of the AGWO-SVM combustion characteristic prediction algorithm established based on the simulation results of the additional five-capacity boilers is improved. Similarly to the 600 MW S-CO_2 CFB boiler, the 1000 MW one consists of an annular furnace core structure with eight cyclones arranged centrosymmetrically around the outer ring. The height, width, and depth of the furnace are 52, 33, and 22 m for the outer ring, respectively, and the dimensions for the furnace inner ring are 19.8 and 10.5 m, respectively. The platen heating surfaces, whose height is 26 m in total, are arranged symmetrically around the inner ring wall. The total air flow rate is 2,315,950 Nm^3/h with the excess air ratio of 1.2 and the temperature of 500 °C. The diameter of coal particles distributes normally varying from 0.7 to 0.8 mm with the coal feeding rate of 296,500 kg/h. The bed material mainly consists of silicon, which also consists of wide sieve particles with the diameter ranging from 0.2 to 0.3 mm.

3.2. AGWO-SVM Prediction Model. Combustion characteristics of the S-CO_2 CFB boiler are studied based on the AGWO-SVM prediction model with the process of the prediction model shown in Figure 5, which is divided into the following five steps:

Step 1: The AGWO-SVM model is constructed.

Step 2: 500 sets of simulation data of the 100 MW S-CO_2 CFB boiler are selected as the training database, which includes operation parameters, boiler size parameters, and combustion characteristic parameters from boiler start to stable operation and is sorted depending on the time series.

Step 3: 300 sets of 0.1, 10, 300, and 600 MW S-CO_2 CFB boilers are respectively selected into the test database. The operating parameters and size parameters in the whole process from boiler start to stable operation are input according to the time series with the boiler combustion characteristic parameter output.

Step 4: The test output results of each capacity boiler are compared with the simulation results. If the difference is within the range of error accepted, the predicted combustion characteristics can output based on the constructed AGWO-SVM prediction model. Otherwise, the test will be repeated.

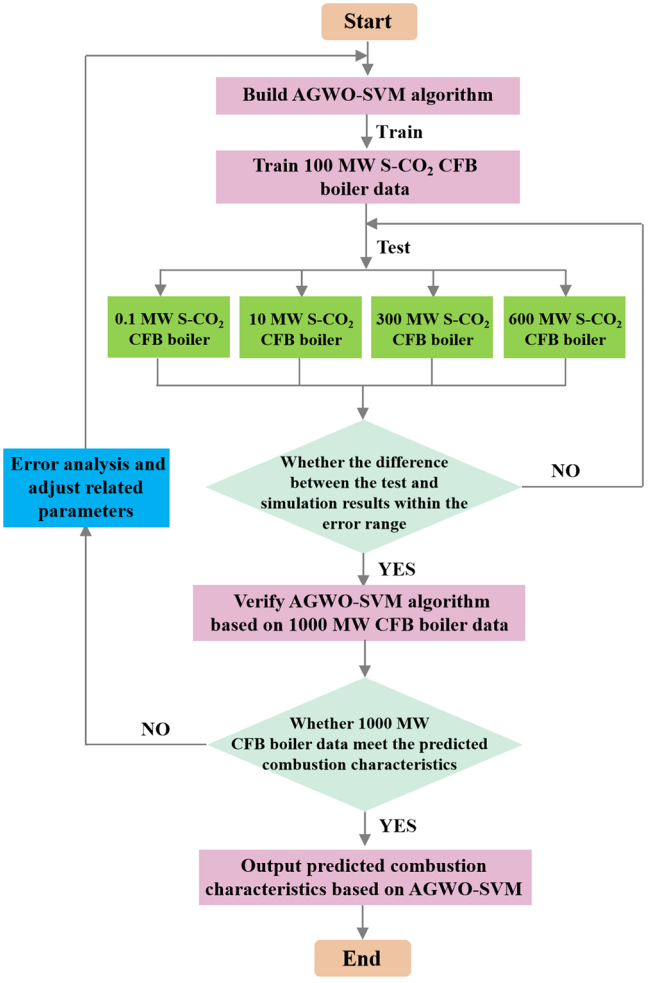

Figure 5. Prediction process of combustion characteristics based on AGWO-SVM.

Step 5: Predicted combustion characteristics are verified based on simulation data of the 1000 MW S-CO_2 CFB boiler. If the 1000 MW S-CO_2 CFB boiler data concur with the predicted combustion characteristic parameters within the set maximum error, the predicted combustion characteristics based on the AGWO-SVM algorithm can be obtained. Otherwise, the AGWO-SVM algorithm should be rebuilt after the error analysis and the adjustment of operating parameters.

The AGWO-SVM network structure diagram is illustrated in Figure 6, which consists of three core parts, namely, input layer, output layer, and hidden layer. The combustion characteristics are determined by numerous parameters of S-CO_2 CFB boilers, not only affected by coal-fired situations such as coal components, diameter distribution, and combustion intensity but also influenced by oxygen abundance, air temperature, dense-phase temperature, excess air coefficient, and wall heat transfer effect. The parameters largely affecting the combustion characteristics should be found and input in the process of modeling and simulation, which can avoid shocking the prediction result data or affecting the accuracy of the predicted combustion characteristics, and the Pearson correlation analysis method is employed. The parameters most closely related to boiler combustion

https://doi.org/10.1021/acsomega.2c07483
ACS Omega 2023, 8, 10160−10175

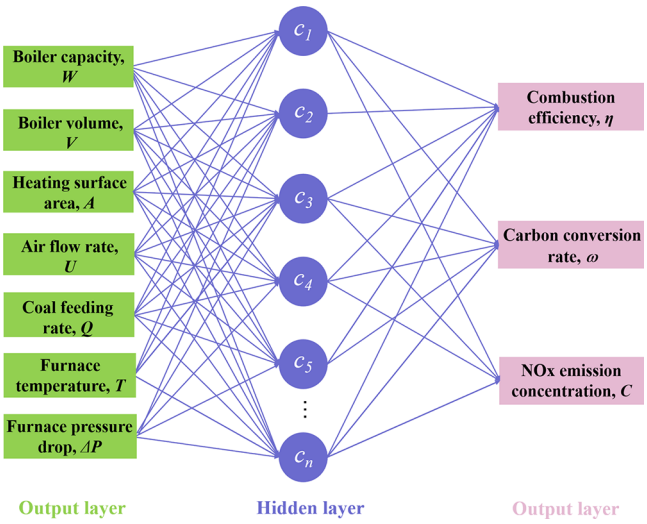

Figure 6. AGWO-SVM network structure diagram.

characteristics are taken as input data, namely, boiler capacity W, boiler volume V, furnace heating surface area A, air flow rate U, coal feeding rate Q, furnace average temperature T, and furnace pressure drop ΔP. Parameters characterizing the combustion characteristics including combustion efficiency η, carbon conversion rate ω, and NO_x emission concentration C are chosen as output data. Table 2 lists some of the input and output operating parameters. There is no detailed research so far on how to determine the optimal number nodes in the hidden layer of the neural network structure, which plays a key role on the training time and prediction performance. Specifically, if the hidden layer node number is set reasonably, the prediction accuracy of the model will be greatly improved. Too few nodes can hinder the progress of the accurate prediction process, and models without making an accurate prediction have no research value. On the contrary, too many hidden layer nodes will increase the training time of the model greatly as the iteration proceeds and the final prediction effect may also be not ideal owing to an allergic phenomenon. Inspired by current research, the number of nodes in the hidden layer is basically selected according to the historical data analysis method. Therefore, in this study, the most appropriate number of hidden layers is constantly explored with only one hidden layer selected as the final neural network subject investigated, which can make excellent predicted results.

3.3. Workflow of the Methodology Overview. The workflow of the methodology overview in this study is shown in Figure 7. First, the gas−solid combustion process of the full-loop S-CO_2 CFB boilers with the capacity varying from 0.1 to 600 MW is simulated to obtain thorough combustion characteristics and change regularities with the increase of the boiler capacity. Second, the AGWO-SVM prediction model is established. The simulated data including boiler capacity, air flow rate, furnace temperature, and coal feeding rate is set as the input data, and the parameters characterizing combustion characteristics including combustion rate, carbon conversion rate, and NO_x emission concentration are chosen as output data. Third, the combustion simulation of the 1000 MW S-CO_2 CFB boiler is conducted to get new operating parameters and combustion characteristic data results. Combustion characteristic data are compared with the prediction results to verify the accuracy of the prediction results. The core research contents are to finish combustion characteristic prediction of the S-CO_2 CFB boiler based on the novel AGWO-SVM model and to get prediction results with higher accuracy compared with conventional SVM and GWO-SVM prediction models.

4. RESULTS AND DISCUSSION

4.1. Simulation Results of Combustion Characteristics. After the establishment of the 3D physical model of the 1000 MW S-CO_2 CFB boiler mentioned in Section 3.1, the full-loop gas−solid combustion process is simulated based on multiphase particle in-cell (MP-PIC) scheme coupling chemical reaction models introduced specifically for the authors' previous research.[11] Detailed combustion characteristics including furnace temperature distribution, gas emission concentration distribution (CO_2, CO, NO, and N_2O) are compared with those of other five boilers to enrich the research of the combustion characteristics in industrial-scale S-CO_2 CFB boilers. Besides, some key parameters representing combustion characteristics are also calculated like the carbon conversion rate ($\omega_{C\text{-}CO2}$), combustion efficiency (η), and NO_x emission concentration (C) to verify the accuracy of the combustion characteristic change regularity.

The CO_2 and CO emission concentrations at the furnace outlet of the 1000 MW S-CO_2 CFB boiler are obtained by simulation. Calculated using eq 22, the carbon conversion rate ($\omega_{C\text{-}CO2}$) of the 1000 MW S-CO_2 CFB boiler is 95.78%, where $M_{CO2\text{-}C}$, $\omega_{coal\text{-}C}$, and Q indicate the mass of C in gas CO_2, the mass fraction of C in coal, and coal feeding rate, respectively.

$$\omega_{C\text{-}CO_2} = \frac{M_{CO_2\text{-}C}}{Q \times \omega_{coal\text{-}C}} \quad (22)$$

The carbon conversion rate fitting curve with the increase of the boiler capacity is given in Figure 8a. The value of the carbon conversion rate of the 1000 MW S-CO_2 CFB boiler is compared with the fitting curve, and it is found that the value coincides well with the fitting curve with the relative error not exceeding 5.2%, proving that the simulated carbon conversion rate fitting formula has acceptable accuracy and application value. The concentration distribution of CO_2 and CO is illustrated in Figure 8b and c, respectively. The concentration distribution of the two gases indicates similar regularity. For industrial-scale S-CO_2 CFB boilers, especially 1000 MW, CO accumulates the most obviously near the coal feeding inlets and drops the fastest along the height of the furnace, which is because industrial-scale boilers will release more volatile content and the rate of CO_2 reduction reaction is the fastest.

According to the simulation results by the authors' previous research,[11] the carbon conversion rate scale-up fitting formula is calculated. In order to improve the accuracy of the carbon conversion scale-up fitting formula, the value of the 1000 MW S-CO_2 CFB boiler is brought into the formula with the updated fitting formula of the carbon conversion rate listed in eq 23.[40] The correction coefficients γ_1, γ_2, and γ_3 are added to the modified formula based on simulation data of the 1000 MW S-CO_2 CFB boiler, where D represents thermal input; α_1, β_1, and γ_1 are 92.66, 497.3, and 1055, respectively; α_2, β_2, and γ_2 are 5.88, 30.05, and 28.94, respectively; α_3, β_3, and γ_3 are 10.222, 108.7, and 119.5, respectively; and γ_1, γ_2, and γ_3 are 1.945, 1.083, and 0.977, respectively.

https://doi.org/10.1021/acsomega.2c07483
ACS Omega 2023, 8, 10160−10175

Table 2. Parts of the CFD Simulation Data in the Database

case	boiler capacity W/MW	boiler volume V/m^3	heating surface area A/m^2	air flow rate U/(kg/s)	coal feeding rate Q/(kg/s)	furnace temperature T/K	furnace pressure ΔP/MPa
A1	0.1	0.1095	2.9202	0.00448	0.0049	1204	46,256
A2	0.1	0.1095	2.9202	0.00425	0.0051	1203	46,311
⋮	⋮	⋮	⋮	⋮	⋮	⋮	⋮
A300	0.1	0.1095	2.9202	0.00401	0.4889	1205	46,279
B1	10	224.3	275.656	0.436	0.5002	1206	45,986
B2	10	224.3	275.656	0.390	0.4895	1195	46,004
⋮	⋮	⋮	⋮	⋮	⋮	⋮	⋮
B300.	10	224.3	275.656	0.408	0.4890	1202	45,799
C1	100	3024	1368	12.17	14.702	1199	45,099
C2	100	3024	1368	12.06	14.697	1195	45,167
⋮	⋮	⋮	⋮	⋮	⋮	⋮	⋮
C500.	100	3024	1368	11.98	14.703	1190	45,233
D1	300	9360	2800	29.23	35.536	1188	44,795
D2	300	9360	2800	28.99	35.557	1197	44,699
⋮	⋮	⋮	⋮	⋮	⋮	⋮	⋮
D300.	300	9360	2800	29.14	35.579	1185	44,756
E1	600	29,346	8760	59.04	72.108	1190	42,854
E2	600	29,346	8760	61.23	72.116	1183	43,757
⋮	⋮	⋮	⋮	⋮	⋮	⋮	⋮
E300.	600	29,346	8760	59.56	72.121	1179	42,967

Case	Combustion rate η/%	Carbon conversion rate ω/%	NO_x emission concentration C/ppmv
A1	91.72	88.35	195.56
A2	90.96	89.39	196.23
⋮	⋮	⋮	⋮
A300	91.14	89.24	197.71
B1	91.45	90.51	198.81
B2	92.04	91.09	199.75
⋮	⋮	⋮	⋮
B300	91.78	9123	199.76
C1	92.73	93.67	183.45
C2	93.25	95.14	186.89
⋮	⋮	⋮	⋮
C500	93.77	95.88	185.95
D1	94.14	96.43	183.53
D2	94.27	96.22	182.22
⋮	⋮	⋮	⋮
D300	94.44	96.67	181.73
E1	94.67	96.78	178.42
E2	94.89	96.57	176.51
⋮	⋮	⋮	⋮
E300	95.03	96.60	177.43

$$\omega_{\text{C-CO}_2} = \gamma_1\alpha_1\exp\left(-\left(\frac{D-\beta_1}{\gamma_1}\right)^2\right) + \gamma_2\alpha_2\exp\left(-\left(\frac{D-\beta_2}{\gamma_2}\right)^2\right) + \gamma_3\alpha_3\exp\left(-\left(\frac{D-\beta_3}{\gamma_3}\right)^2\right) \quad (23)$$

The gas phase temperature and solid phase temperature distributions of the 1000 MW S-CO_2 CFB boiler are obtained by numerical simulation, and the combustion efficiency is calculated using eqs 24−27.[41]

$$\eta = 100 - q_3 - q_4 \quad (24)$$

$$q_3 = \frac{1}{Q_r}V_{gy}(126.36CO + 358.18CH_4 + 107.98H_2) \times 100 \quad (25)$$

$$q_4 = q_4^{FA} = \frac{Q_c G_{c\text{-FA}}}{Q_{net,ar}} \quad (26)$$

$$G_{C\text{-FA}} = G_{C\text{-Fuel}} - G_{C\text{-Unburn}} - G_{C\text{-Gas}} \quad (27)$$

where Q_r is the thermal input to the furnace and V_{gy} is the volume of the dry flue gas generated per kg of fuel combustion. q_4^{FA} represents the fly ash heat loss, and the bottom slag heat loss is omitted because any slag discharge system is included in the simulation of the S-CO_2 CFB boiler. $Q_{net,ar}$ and Q_c represent the net calorific value as received basis and the carbon heating value, respectively. $G_{C\text{-FA}}$, $G_{C\text{-Fuel}}$, $G_{C\text{-Unburn}}$, and $G_{C\text{-Gas}}$ represent the carbon mass in the fly ash, fuel input, unburned fuel, and the produced gas containing C, respectively.

The combustion efficiency value of the 1000 MW S-CO_2 CFB boiler is compared with the fitting curve, as displayed in Figure 9a. The point representing the 1000 MW boiler

https://doi.org/10.1021/acsomega.2c07483
ACS Omega 2023, 8, 10160−10175

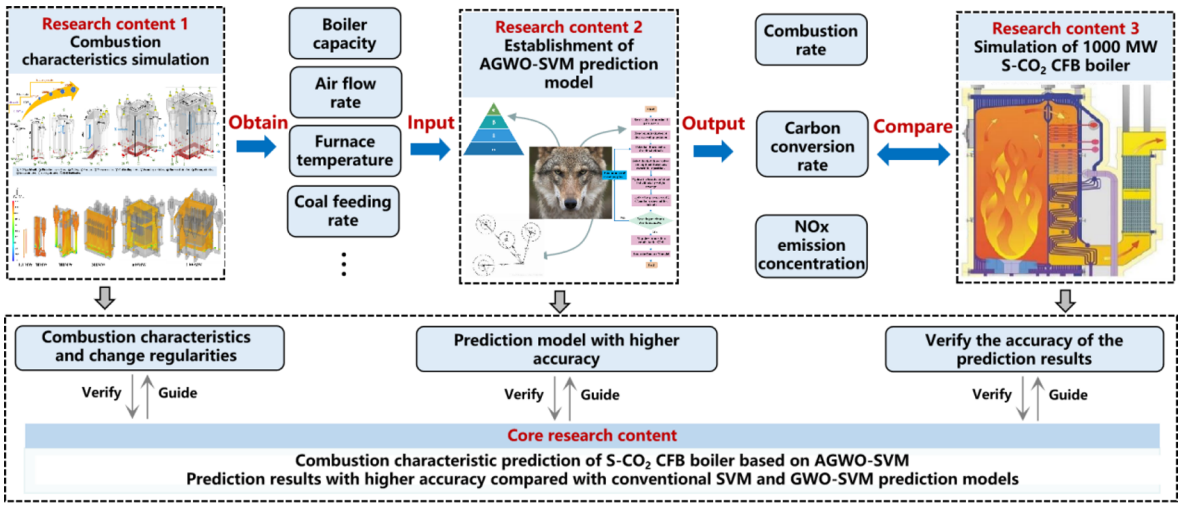

Figure 7. Workflow of the methodology overview.

combustion efficiency (94.23%) falls right on the fitting curve, which is just slightly lower than the curve with the maximum deviation of no more than 6.78%. This phenomenon suggests that the change regularity of the combustion efficiency obtained by S-CO_2 CFB boilers with capacities varying from 0.1 to 600 MW is accurate. The furnace temperature distribution of the six S-CO_2 CFB boilers is illustrated in Figure 9b. With the increase of thermal input, the gas phase temperature of the furnace shows an overall downward trend and the average temperatures are 1201, 1198.2, 1190.5, 1186.4, 1183.5, and 1182.9 K, respectively. Among them, the temperature of laboratory-scale (0.1 MW) and pilot-scale (10 MW) boilers is particularly affected by coal feeding and secondary air input, while industrial-scale boilers with more uniform temperature distributions (100, 300, 600, 1000 MW) are less affected. Higher temperature helps to improve the combustion efficiency, and more uniform temperature distribution favors combustion uniformity and stability.

In order to further improve the accuracy of the change regularity of combustion efficiency, the numerical simulation data of the 1000 MW S-CO_2 CFB boiler is also taken into account in the proposal of the fitting formula, which makes it more consistent with reality by adding the correction coefficient. The modified combustion efficiency scale-up fitting formula is shown in eq 2828, where correction coefficients γ_1, γ_2, and γ_3 and are 0.984, 1.221, and 0.797, respectively.

$$\eta = \kappa_1 X_1 \exp\left(-\left(\frac{D - Y_1}{Z_1}\right)^2\right) + \kappa_2 X_2 \exp\left(-\left(\frac{D - Y_2}{Z_2}\right)^2\right) + \kappa_3 X_3 \exp\left(-\left(\frac{D - Y_3}{Z_3}\right)^2\right) \quad (28)$$

Similar to the exploration of the carbon conversion rate and combustion efficiency discussed above, the NO and N_2O concentration distribution in the 1000 MW S-CO_2 CFB boiler furnace is obtained by numerical simulation, as shown in Figure 10. Data points representing the NO_x emission concentration of the 1000 MW S-CO_2 CFB boiler agree with the deduced NO_x emission concentration fitting curve with the increase of the boiler capacity with the relative error of 7.32%, verifying its accuracy with acceptable precision. Figure 10b and c show the concentration distribution of NO and N_2O in the full-loop six-capacity boilers. Because the coal content of industrial-scale S-CO_2 CFB boilers is the highest, especially for the 1000 MW one, more coal reacts with NO, which advances the consumption of NO, so the NO concentration of industrial-scale boilers is lower. The N_2O concentration of industrial-scale S-CO_2 CFB boilers is high because the concentration of CO in the furnace is too low to convert excess N_2O.

The NO_x emission concentration value of 1000 MW S-CO_2 CFB boiler (182.7 ppmv) is brought in to the obtained fitting curve of the NO_x emission change regularity to improve the accuracy of the representation. The modified scale-up fitting formula is listed in eq 29 with the correction coefficients ζ_1, ζ_2, ζ_3, and ζ_4 of 1.022, 0.996, 1.115, and −0.0009, respectively.

$$C = \zeta_1 X_1 W^3 + \zeta_2 X_2 W^2 + \zeta_3 X_3 W + \zeta_4 X_4 \quad (29)$$

4.2. Prediction Results of Combustion Characteristics. In order to verify the effect of the S-CO_2 CFB combustion characteristic prediction model of AGWO-SVM established in this study, it is compared with the conventional GWO-SVM prediction model and the SVM prediction model. The comparative prediction results of the 600 MW S-CO_2 CFB boiler combustion efficiency based on each model are the most representative, as shown in Figure 11a–c. Figure 11d shows the prediction error of the three prediction models. It is noted that the GWO-SVM and AGWO-SVM prediction models fit quite well with the prediction accuracy improved to varying degrees compared with the conventional SVM prediction model. The relative error of the maximum pulsation amplitude (δ_{max}) of the AGWO-SVM prediction model is the smallest of the three models (1.02%), and the number of mismatch point pairs is much fewer than the other two algorithms. On the one hand, this regularity reflects that GWO algorithms have better power in searching for the optimal parameters. On the other hand, the novel AGWO-SVM prediction model corresponding to the S-CO_2 CFB boiler can better reflect the changing trend of combustion efficiency in the boiler combustion process and obtain more ideal combustion characteristics and regularity prediction results, which has an excellent guiding significance for adjusting parameters of industrial-scale S-CO_2 CFB boilers in real time.

https://doi.org/10.1021/acsomega.2c07483
ACS Omega 2023, 8, 10160−10175

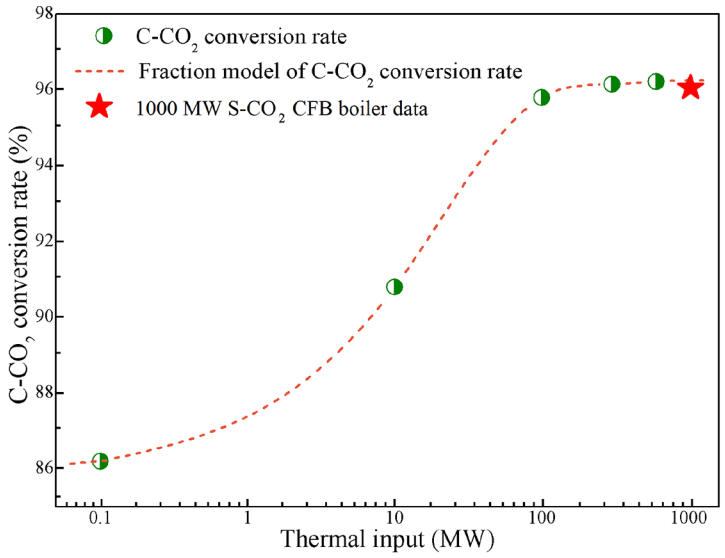

(a)

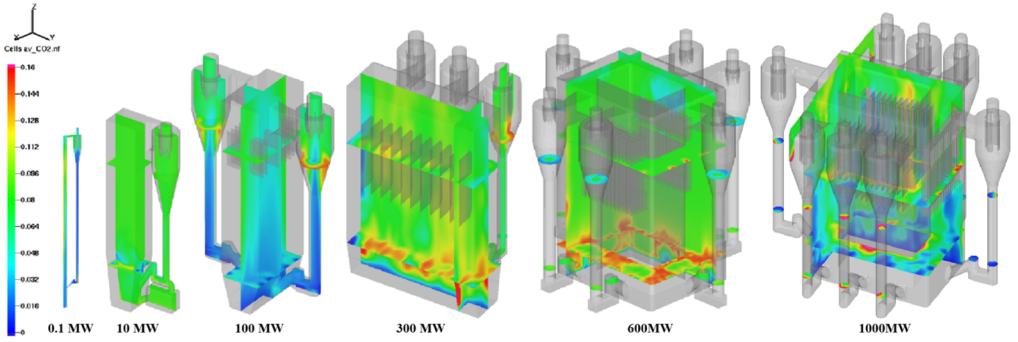

(b)

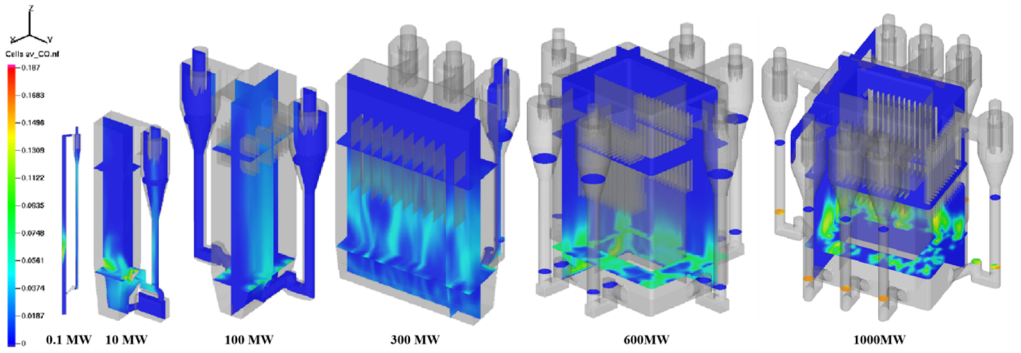

(c)

Figure 8. C-CO_2 conversion rate verification by the 1000 MW S-CO_2 CFB boiler: (a) C-CO_2 conversion rate scale-up fitting curve, (b) CO_2 concentration distribution in six-capacity boilers, and (c) CO concentration distribution in six-capacity boilers.

The comparison of prediction and results simulation on the boiler carbon conversion rate is shown in Figure 12a−c. Figure 12d presents the corresponding prediction error. Compared with the conventional GWO-SVM prediction model, the AGWO-SVM prediction model obtains the carbon conversion prediction curve fitting the best with the simulation curve, with the matching points significantly reduced compared with the other two algorithms. Meanwhile, the mismatching rate dramatically declines, indicating a better prediction ability. The relative error of the AGWO-SVM prediction model is under 0.75%, which is less than that of the GWO-SVM prediction model and the SVM prediction model, whose relative errors are 1.34 and 2.56%, respectively. The prediction results can also be a useful response to actual changing trends especially in some situations when the fluctuation of the furnace working conditions is relatively larger. This is because the AGWO algorithm adjusts the inertial weight for chaotic inertia, the learning factor is adaptively processed, and the particles perform cross-variation operations. In this case, the ability of the AGWO algorithm is strengthened and the

https://doi.org/10.1021/acsomega.2c07483
ACS Omega 2023, 8, 10160−10175

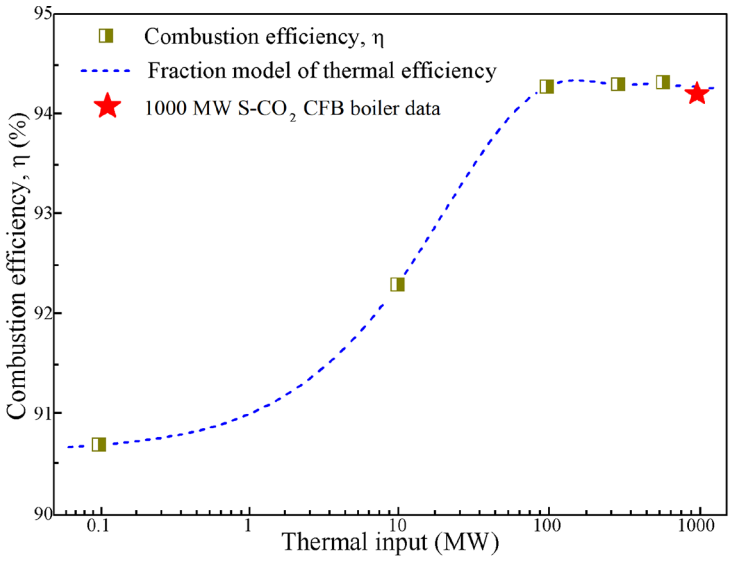

(a)

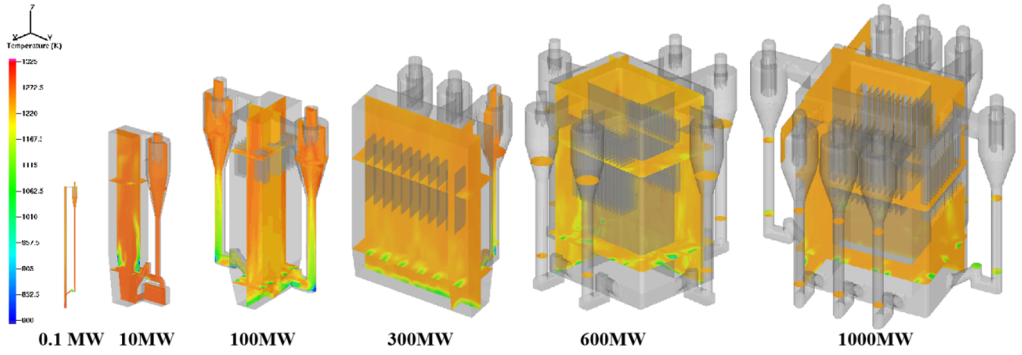

(b)

Figure 9. Combustion efficiency verification by the 1000 MW S-CO_2 CFB boiler: (a) combustion efficiency scale-up fitting curve and (b) combustion distribution in six capacity boilers.

prediction accuracy of the combustion characteristics of S-CO_2 CFB boilers is improved.

Figure 13a–c shows the comparison of the prediction results of the boiler NO_x emission concentration and simulation data, and the prediction errors of the three prediction models are presented in Figure 13d. It is seen that the prediction results of the three models are relatively stable with a relative error within 10%. Among the three prediction models, the AGWO-SVM algorithm best agrees with the simulated value, whose relative error does not exceed 5.61%, indicating a quite high accuracy in the NO_x emission prediction of the S-CO_2 CFB boiler. The SVM prediction model indicates the largest relative error of 9.23%, and the predictive ability of the GWO-SVM prediction model is somewhere in between with the relative error of 8.74%. The fitting degree of the AGWO-SVM algorithm predicting NO_x emission is slightly less than that predicting the combustion efficiency and carbon conversion rate, but the overall effect is satisfactory. Results show that the generalization time and pattern recognition accuracy of the AGWO-SVM algorithm model have great advantages, which are competent for the prediction work and have fine stability. Overall, the novel AGWO-SVM algorithm is an effective method to predict the parameters related to the combustion characteristics of the S-CO_2 CFB boiler.

Three sets of critical data representing the combustion characteristic parameters after the final output of the above three prediction models, namely, the combustion efficiency, carbon conversion rate, and NO_x emission concentration, are compared with the original simulation data. The comparison results are presented in Table 3. According to the table, the combustion efficiency, carbon conversion rate, and NO_x emission of the AGWO-SVM prediction model proposed in this study are 96.78%, 94.56%, and 188.760 ppmv, which are the closest to the original numerical simulation results (96.55%, 94.76%, and 189.332 ppmv), with the error not exceeding 0.85%, while the data obtained by the SVM model differ greatly from the original data and the prediction results obtained by the GWO-SVM prediction model are in between. Besides, the AGWO-SVM prediction model presented in this study optimizes combustion characteristic data of boilers to obtain a higher combustion efficiency and carbon conversion rate, as well as a lower NO_x emission concentration, indicating that the AGWO-SVM prediction model has an excellent prediction and optimization effect.

https://doi.org/10.1021/acsomega.2c07483
ACS Omega 2023, 8, 10160−10175

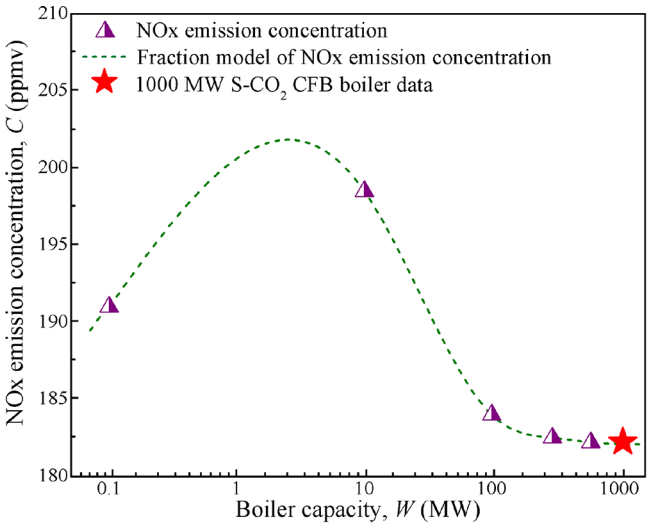

(a)

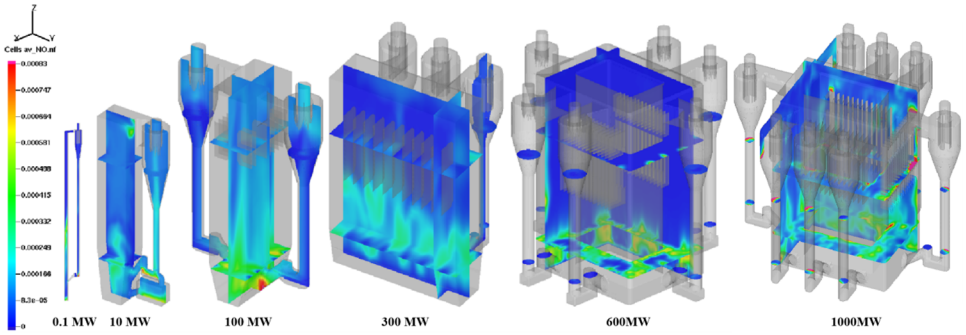

(b)

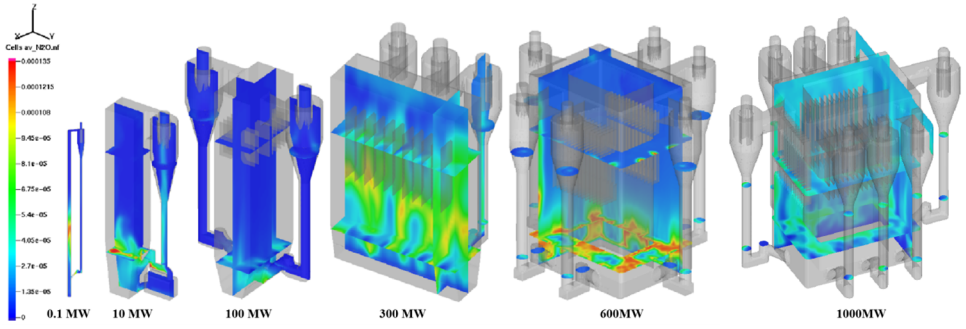

(c)

Figure 10. NO_x emission concentration verification by the 1000 MW S-CO_2 CFB boiler: (a) NO_x emission concentration scale-up fitting curve, (b) NO concentration in six-capacity boilers, and (c) N_2O concentration in six-capacity boilers.

5. CONCLUSIONS

A novel AGWO-SVM algorithm is proposed in this study to further improve the performance of combustion characteristic prediction models for S-CO_2 CFB boilers. This new prediction model solves the imbalance of local and global search abilities in the conventional GWO algorithm, and the dynamic weights are introduced to accelerate the algorithm convergence, which can realize accurate combustion characteristics of the S-CO_2 CFB boiler with high industrial application value. The main findings are as follows:

(1) In the CFD numerical simulation, the MP-PIC method and coal combustion model are used to simulate the gas−solid flow and combustion process of the 1000 MW S-CO2 CFB boiler, the calculation results are compared with the data rule of the previous research, and the errors on the carbon conversion rate, combustion efficiency, and NO_x emission concentration is less than 7.32%. Besides, the addition of 1000 MW S-CO_2 CFB boiler test data optimizes the proposed AGWO-SVM prediction model.

(2) By establishing the novel AGWO-SVM algorithm, the combustion characteristic and change regularities with boiler capacities of 0.1, 10, 100, 300, 600, and 1000 MW are predicted with acceptable accuracy. The AGWO-

https://doi.org/10.1021/acsomega.2c07483
ACS Omega 2023, 8, 10160−10175

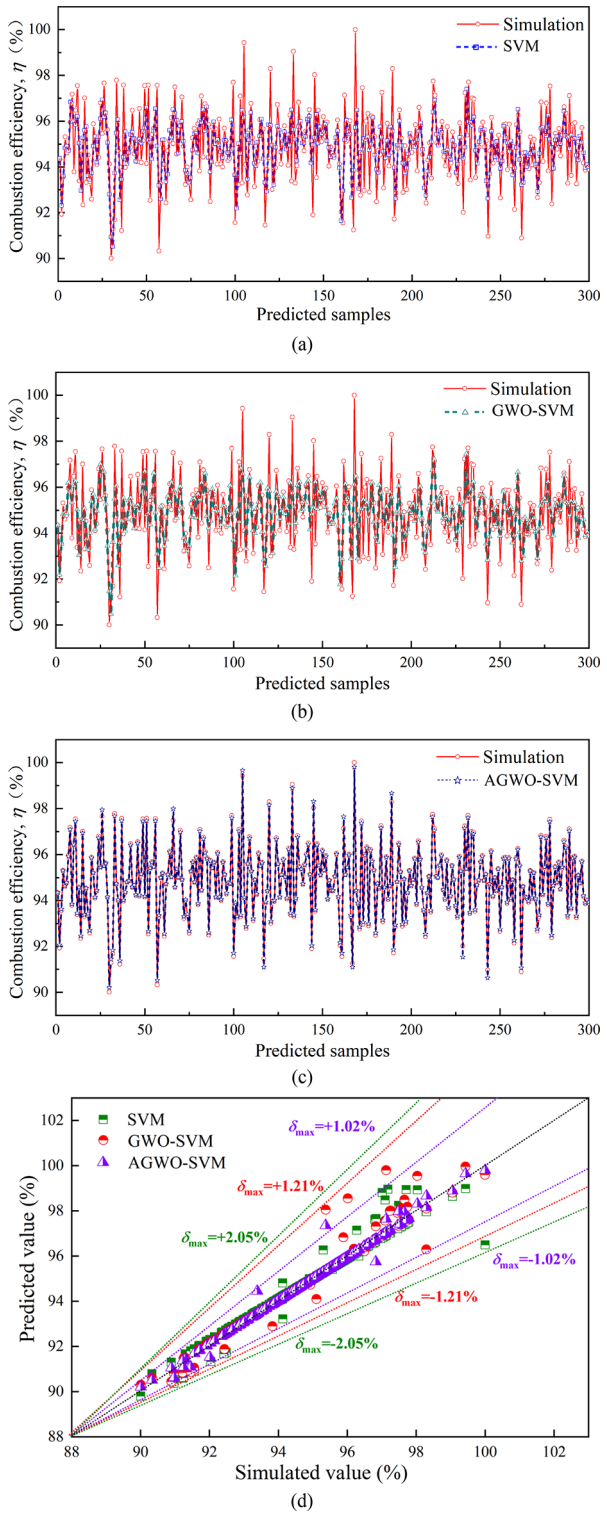

Figure 11. Comparison between prediction and simulation results of combustion efficiency for the 600 MW S-CO_2 CFB boiler: (a) SVM prediction model, (b) GWO-SVM prediction model, (c) AGWO-SVM prediction model, and (d) prediction error.

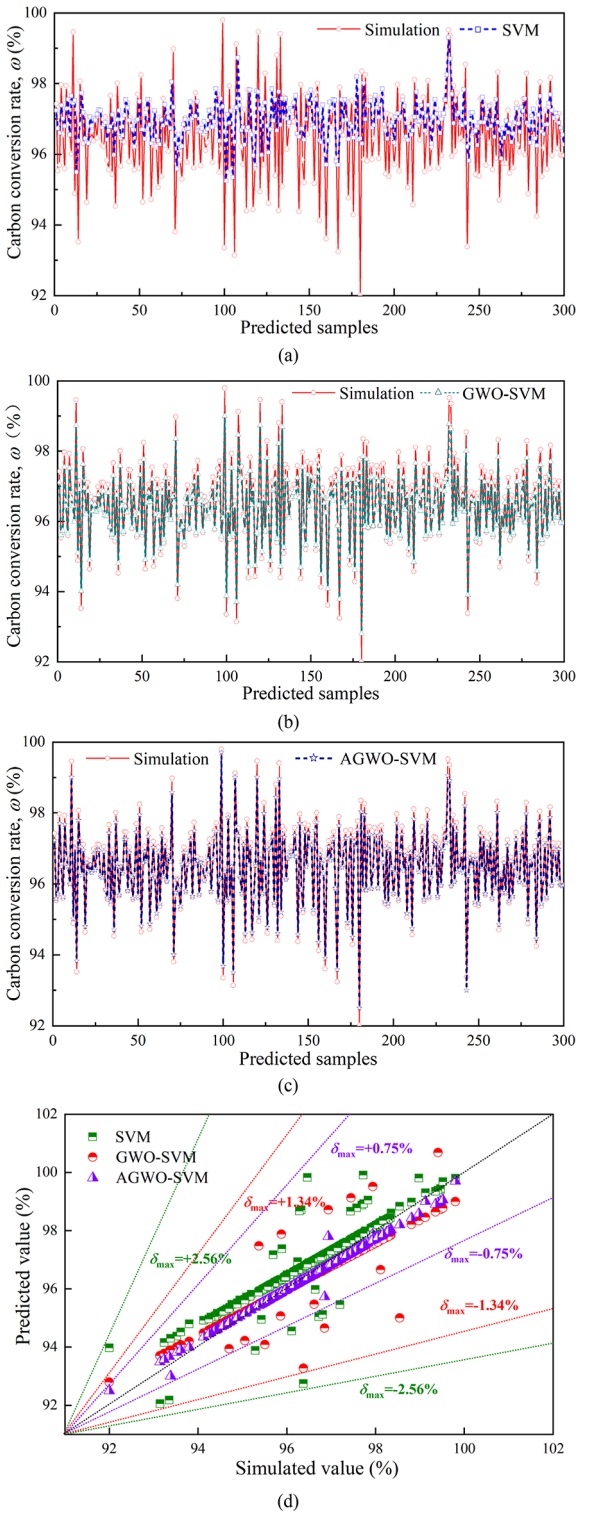

Figure 12. Comparison between prediction and simulation results of the carbon conversion rate for the 600 MW S-CO_2 CFB boiler: (a) SVM prediction model, (b) GWO-SVM prediction model, (c) AGWO-SVM prediction model, and (d) prediction error.

SVM prediction relative errors on combustion efficiency, carbon conversion rate, and NO_x emission concentration are 1.02, 0.75, and 5.61%, respectively, compared with simulation data.

(3) Compared with the conventional GWO-SVM and SVM prediction models, the combustion efficiency, carbon conversion rate, and NO_x emission concentration of the 600 MW S-CO_2 CFB boiler obtained based on the AGWO-SVM algorithm best agree with the simulated data with mismatch points less than the other two algorithms, and the relative error of the pulsation maximum amplitude does not exceed 6%. The proposed

https://doi.org/10.1021/acsomega.2c07483
ACS Omega 2023, 8, 10160−10175

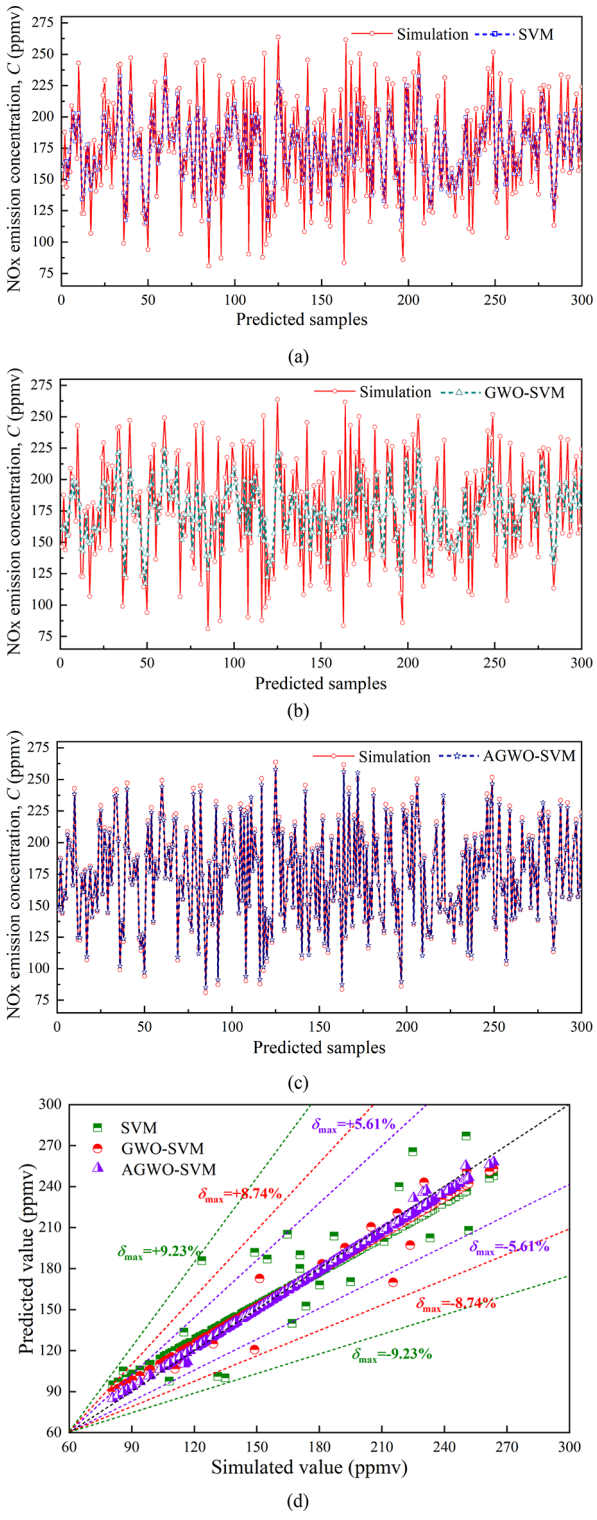

Figure 13. Comparison between prediction and simulation results of the NO_x emission concentration for the 600 MW S-CO_2 CFB boiler: (a) SVM prediction model, (b) GWO-SVM prediction model, (c) AGWO-SVM prediction model, and (d) prediction error.

novel AGWO-SVM algorithm improves the reliability and the prediction accuracy of the combustion characteristics of the S-CO_2 CFB boiler.

Table 3. Main Combustion Characteristic Parameters of Compared Experiment Based on Original Data and the Adaptive Method

	original simulation data	SVM	GWO-SVM	AGWO-SVM
combustion efficiency (%)	96.55	89.43	92.31	97.38
carbon conversion rate (%)	94.76	86.74	90.23	95.56
NO_x emission concentration (ppmv)	189.332	213.565	197.843	188.760

AUTHOR INFORMATION

Corresponding Authors

Ying Cui − *School of Automotive and Transportation, Wuxi Institute of Technology, Wuxi, Jiangsu Province 214000, P.R. China; Key Laboratory of Energy Conversion and Process Measurement and Control Ministry of Education, School of Energy and Environment, Southeast University, Nanjing, Jiangsu Province 210096, P.R. China; ARC Research Hub for Computational Particle Technology, Department of Chemical Engineering, Monash University, Clayton, Victoria 3800, Australia;* orcid.org/0000-0003-0802-6793; Phone: +86-15951573926; Email: cuiy@wxit.edu.cn

Wenqi Zhong − *Key Laboratory of Energy Conversion and Process Measurement and Control Ministry of Education, School of Energy and Environment, Southeast University, Nanjing, Jiangsu Province 210096, P.R. China; Centre for Simulation and Modelling of Particulate Systems, Southeast University-Monash University Joint Research Institute, Suzhou 215000, PR China;* orcid.org/0000-0003-0700-4592; Phone: +86-25-83794744; Email: wqzhong@seu.edu.cn; Fax: +86-25-83795508

Authors

Ye Zou − *School of Automotive and Transportation, Wuxi Institute of Technology, Wuxi, Jiangsu Province 214000, P.R. China*

Shujun Jiang − *School of Automotive and Transportation, Wuxi Institute of Technology, Wuxi, Jiangsu Province 214000, P.R. China*

Complete contact information is available at: https://pubs.acs.org/10.1021/acsomega.2c07483

Notes

The authors declare no competing financial interest.

ACKNOWLEDGMENTS

Financial support from the National Key Research and Development Program of China (no. 2017YFB0601802) and the Key Research and Development Program of Jiangsu Province (no. BE2017159) is sincerely acknowledged.

NOMENCLATURE

AGWO-SVM adaptive gray wolf optimizer support vector machine
EHE external heat exchanger
ESE evolutionary state estimation
IGWO-ELM improved gray wolf optimizer extreme learning machine
LS-SVM least-square support vector machine

https://doi.org/10.1021/acsomega.2c07483
ACS Omega 2023, 8, 10160−10175

GWO gray wolf optimizer
a convergence factor
A furnace heating surface area (m^2)
A' coefficient vector
b constant
C NO_x emission concentration
C' coefficient vector
C'' penalty coefficient
D thermal input (MW)
K radial base nuclear function
k number of cyclic iterations
L fitness value
M mass (kg)
n particle number
Q coal feeding rate (kg/s)
Q_r thermal input to the furnace (kJ/kg)
Q_c carbon heating value (kJ/kg)
$Q_{net,ar}$ thermal input of the coal (kJ/kg)
q_3 combustible gases incomplete combustion heat loss (%)
q_4 solid fuels incomplete combustion heat loss (%)
q_4^{FA} efficiency loss related with the fly ash (%)
r random quantity between 0 and 1
t number of iterations
T furnace average temperature (K)
U air flow rate (kg/s)
V boiler volume (m^3)
V_{gy} volume of the dry flue gas (m^3)
v particle velocity
v_{i1} initial velocity
W boiler capacity (MW)
x location in space (m)
x_{i1} initial position
X positions of wolf
y location in space (m)

Greek letters

α α wolf
β β wolf
δ δ wolf
σ radial basis parameter
η combustion efficiency
ω carbon conversion rate
δ_{max} elative error of maximum pulsation amplitude
ξ relaxation variable
γ carbon conversion rate correction coefficient
γ combustion efficiency correction coefficient
ζ NO_x emission concentration correction coefficient

REFERENCES

(1) Li, H.; Zhang, Y.; Yang, Y.; Han, W.; Yao, M.; Bai, W.; Zhang, L. Preliminary Design Assessment of Supercritical CO_2 Cycle for Commercial Scale Coal-fired Power Plants. *Appl. Therm. Eng.* **2019**, *158*, 1−10.
(2) Yu, A.; Su, W.; Lin, X.; Zhou, N. Recent trends of supercritical CO_2 Brayton cycle: Bibliometric analysis and research review. *Nucl. Eng. Technol.* **2021**, *53*, 699−714.
(3) White, M. T.; Bianchi, G.; Chai, L.; Tassou, S. A.; Sayma, A. I. Review of supercritical CO_2 technologies and systems for power generation. *Appl. Therm. Eng.* **2021**, *185*, No. 116447.
(4) Liu, X.; Zhang, M.; Zhang, S.; Ding, Y.; Huang, Z.; Zhou, T.; Yang, H.; Yue, G. Measuring Technologies for CFB Solid Circulation Rate: A Review and Future Perspectives. *Energies* **2022**, *15*, 417.
(5) Castilla, G. M.; Montañés, R. M.; Pallarès, D.; Johnsson, F. Comparison of the Transient Behaviors of Bubbling and Circulating Fluidized Bed Combustors. *Heat Transf. Eng.* **2023**, 303.
(6) Koornneef, J.; Junginger, M.; André, F. Development of Fluidized Bed Combustion- An Overview of Trends, Performance and Cost. *Prog. Energy Combust.* **2007**, *33*, 19−55.
(7) Chen, J.; Yang, T.; Li, D.; Li, J.; Han, C.; Yu, G.; Zhao, C.; Liu, X. Evaluation of direct quadrature method of moment for the internally circulating fluidized bed simulation with ultrafine particles. *Adv. Powder Technol.* **2021**, *32*, 2359−2369.
(8) Mecheri, M.; Le Moullec, Y. Supercritical CO_2 Brayton Cycles for Coal-fired Power Plants. *Energy* **2016**, *103*, 758−771.
(9) Xu, J.; Sun, E.; Li, M.; Liu, H.; Zhu, B. Key Issues and Solution Strategies for Supercritical Carbon Dioxide Coal Fired Power Plant. *Energy* **2018**, *157*, 227−246.
(10) Li, P.; Zhong, W.; Chen, X.; Liu, X. Heat Distribution and Boiler Efficiency of 600MW Coal-fired CFB Boiler with S-CO_2 Power Cycle. *Proc. CSEE* **2019**, *39*, 2080−2093.
(11) Cui, Y.; Zhong, W.; Liu, X.; Xiang, J. Study on scale-up characteristics in supercritical CO_2 circulating fluidized bed boiler by 3D CFD simulation. *Powder Technol.* **2021**, *934*, 103−119.
(12) Cui, Y.; Zhong, W.; Xiang, J.; Liu, G. Simulation on coal-fired supercritical CO_2 circulating fluidized bed boiler: Coupled combustion with heat transfer. *Adv. Powder Technol.* **2019**, *30*, 3028−3039.
(13) Murat, V.; Aysel, T. A.; Hayati, O. Emission characteristics of co-combustion of a low calorie and high-sulfur-lignite coal and woodchips in a circulating fluidized bed combustor: Part 2. Effect of secondary air and its location. *Fuel* **2014**, *130*, 1−9.
(14) Francesco, C.; Giacomo, G.; David, S. Supercritical carbon dioxide cycles for power generation: A review. *Appl. Energy* **2017**, *195*, 152−183.
(15) Shao, Y.; Liu, X.; Zhong, W.; Jin, B.-S.; Zhang, M. Recent Advances of Spout-Fluid Bed: A Review of Fundamentals and Applications. *Int. J. Chem. React. Eng.* **2013**, *11*, 243−258.
(16) Glicksman, L. R. Scaling relationships for fluidized-beds. *Chem. Eng. Sci.* **1984**, *39*, 1373−1379.
(17) Zhou, J.; Zhang, C.; Su, S.; Wang, Y.; Hu, S.; Liu, L.; Ling, P.; Zhong, W.; Xiang, J. Exergy analysis of a 1000MW single reheat supercritical CO_2 Brayton cycle coal-fired power plant. *Energy Convers. Manage.* **2018**, *173*, 348−358.
(18) Yang, Y.; Bai, W.; Wang, Y.; Zhang, Y.; Li, H.; Yao, M.; Wang, H. Coupled simulation of the combustion and fluid heating of a 300MW supercritical CO_2 boiler. *Appl. Therm. Eng.* **2017**, *113*, 259−267.
(19) Wang, F.; Su, H.; Chen, T.; Yu, Q.; Huang, Y.; Zhang, Y. J.; Shen, T. Coupled modeling of combustion and hydrodynamics for a supercritical CO_2 boiler. *Appl. Therm. Eng.* **2018**, *143*, 711−718.
(20) Gu, J.; Shao, Y.; Zhong, W. Study on oxy-fuel combustion behaviors in a S-CO_2 CFB by 3D CFD simulation. *Chem. Eng. Sci.* **2020**, *211*, No. 115262.
(21) Liu, X.; Zhong, W.; Li, P.; Liu, G. Design and performance analysis of coalfired fluidized bed for supercritical CO_2 power cycle. *Energy* **2019**, *176*, 468−478.
(22) Cai, J.; Ma, X.; Li, Q. On-line monitoring the performance of coal-fired power unit: A method based on support vector machine. *Appl. Therm. Eng.* **2009**, *29*, 2308−2319.
(23) Song, F.; Cheng, G.; Sun, F.; Zhu, G. Reconstruction of key parameters of marine supercharged boiler based on PLS-SVM. *Adv. Mater.* **2014**, *859*, 19−22.
(24) Liu, Q.; Yao, G. Improved coal combustion optimization model based on load balance and coal qualities. *Energy* **2017**, *132*, 204−212.
(25) Zhang, Y.; Zhang, H.; Zhang, W. Optimization of coal-fired boiler on LS-SVM model and GWO algorithms. *Adv. Eng. Res.* **2015**, *32*, 329−334.
(26) Gu, Y.; Zhao, W.; Wu, Z. Combustion optimization for utility boiler based on least square-support vector machine. *Proc. CSEE* **2010**, *30*, 91−97.
(27) Gu, M.; Liu, J. A support vector machine based on an improved particle swarm optimization algorithm for SEMG signal pattern recognition. *Chin. J. Sens. Actuators* **2017**, *30*, 1459−1464.
(28) Wu, H.; Yu, H; Yang, H. Communication protocols realization of the prediction and evaluation light environment embedded

https://doi.org/10.1021/acsomega.2c07483
ACS Omega 2023, 8, 10160−10175

systems. *2010 International Conference on Machine Vision and Human-Machine Interface*; IEEE *2010*, 109—112.
(29) Zhang, X.; Zhang, Y.; Zhou, Y. Measuring and modeling photosynthetically active radiation in Tibet Plateau during April-October. *Agric. For. Meteorol.* **2000**, *102*, 207−212.
(30) Amari, S.; Wu, S. Improving support vector machine classifiers by modifying kernel functions. *Neural Netw.* **1999**, *12*, 783−789.
(31) Gu, J.; Jiang, T.; Zhu, H.; Zhang, C. Low-carbon job shop scheduling problem with discrete genetic-grey wolf optimization algorithm. *J. Manuf. Syst.* **2020**, *19*, 1−4.
(32) Shi, W.; Song, C. Improved grey wolf optimization for solving hybrid flow shop scheduling problem. *CIMS.* **2021**, *27*, 3196−3208.
(33) Zhu, Z.; Zhou, X. An efficient evolutionary grey wolf optimizer for multi-objective flexible job shop scheduling problem with hierarchical job precedence constraints. *Comput. Ind. Eng.* **2020**, *140*, No. 106280.
(34) Sakawa, M.; Mori, T. An efficient genetic algorithm for job-shop scheduling problems with fuzzy processing time and fuzzy duedate. *Comput. Ind. Eng.* **1999**, *36*, 325−341.
(35) Mirjalili, S.; Mirjalili, S. M.; Lewis, A. Grey Wolf Optimizer. *Adv. Eng. Software* **2014**, *69*, 46−61.
(36) Gupta, S.; Deep, K. Enhanced leadership-inspired grey wolf optimizer for global optimization problems. *Eng. Computation* **2020**, *36*, 98−1800.
(37) Devarapalli, R.; Bhattacharyya, B. An intelligent EGWO-SCA-CS algorithm for PSS parameter tuning under system uncertainties. *Int. J. Intell. Syst.* **2020**, *35*, 119−125.
(38) Liu, Y.; Sun, J.; Yu, H.; Wang, Y.; Zhou, X. An Improved grey wolf Optimizer Based on Differential Evoluti on and OTSU Algorithm. *Appl. Sci.* **2020**, *10*, 6343.
(39) Bansal, J. C.; Singh, S. A better exploration strategy in Grey Wolf Optimizer. *J. Ambient. Intell. Humaniz. Comput.* **2021**, *12*, 1099−1118.
(40) *Fired steam generators performance test code, ASME PTC 4−1998*; American Association of Mechanical Engineers 1999.
(41) GB10184−88. *Test Rules for Boiler Performance of Power Station*.

https://doi.org/10.1021/acsomega.2c07483
ACS Omega 2023, 8, 10160−10175